Title

Image-derived Metrics Quantifying Hemodynamic Instability Predicted Growth of Unruptured Intracranial Aneurysms.

Journal

Stroke: Vascular and Interventional Neurology, 3(1)

Authors

Yang, Hong-Ho
Sayre, James
Dinh, Huy
et al.

Publication Date

2023

DOI

10.1161/svin.122.000426

Peer reviewed

HHS Public Access

Author manuscript

Stroke Vasc Interv Neurol. Author manuscript; available in PMC 2023 April 20.

Published in final edited form as:

Stroke Vasc Interv Neurol. 2023 January ; 3(1): . doi:10.1161/svin.122.000426.

Image-derived Metrics Quantifying Hemodynamic Instability Predicted Growth of Unruptured Intracranial Aneurysms

Hong-Ho Yang, BS[1], **James Sayre, PhD**[1], **Huy Dinh, BS**[1], **Kambiz Nael, MD**[1], **Geoffrey Colby, MD, PhD**[2], **Anthony Wang, MD**[2], **Pablo Villablanca, MD**[1], **Noriko Salamon, MD**[1], **Aichi Chien, PhD**[1]

[1]David Geffen School of Medicine at UCLA, Department of Radiology, Los Angeles, California, USA

[2]David Geffen School of Medicine at UCLA, Department of Neurosurgery, Los Angeles, California, USA

Abstract

Background: While image-derived predictors of intracranial aneurysm (IA) rupture have been well-explored, current understanding of IA growth is limited. Pulsatility index (PI) and wall shear stress pulsatility index (WSSPI) are important metrics measuring temporal hemodynamic instability. However, they have not been investigated in IA growth research. The present study seeks to verify reliable predictors of IA growth with comparative analyses of several important morphological and hemodynamic metrics between stable and growing cases among a group of unruptured IAs.

Methods: Using 3D images, vascular models of 16 stable and 20 growing cases were constructed and verified using Geodesic techniques. With an overall mean follow-up period of 25 months, cases exhibiting a 10% or higher increase in diameter were considered growing. Patient-specific, pulsatile simulations were performed, and hemodynamic calculations were computed at 5 important regions of each aneurysm (inflow artery, aneurysm neck, body, dome, and outflow artery). Index values were compared between growing and stable IAs using ANCOVA controlling for aneurysm diameter. Stepwise multiple logistic regression and ROC analyses were conducted to investigate predictive models of IA growth.

Results: Compared to stable IAs, growing IAs exhibited significantly higher intrasaccular PI, intrasaccular WSSPI, intrasaccular spatial flow rate deviation, and intrasaccular spatial wall shear stress (WSS) deviation. Stepwise logistic regression analysis revealed a significant predictive model involving PI at aneurysm body, WSSPI at inflow artery, and WSSPI at aneurysm body.

Conclusions: Our results showed that high degree of hemodynamic variations within IAs is linked to growth, even after controlling for morphological parameters. Further, evaluation of PI in conjunction with WSSPI yielded a highly accurate predictive model of IA growth. Upon

Corresponding Author: Aichi Chien, PhD, Department of Radiology, David Geffen School of Medicine at UCLA, 10833 LeConte Ave, Box 951721, Los Angeles, CA 90095, aichi@ucla.edu.

SUPPLEMENTAL MATERIALS

Expanded Materials & Methods

Appendix 1. Index Formula

validation in future cohorts, these metrics may aid in early identification of IA growth and current understanding of IA remodeling mechanism.

Graphical Abstract

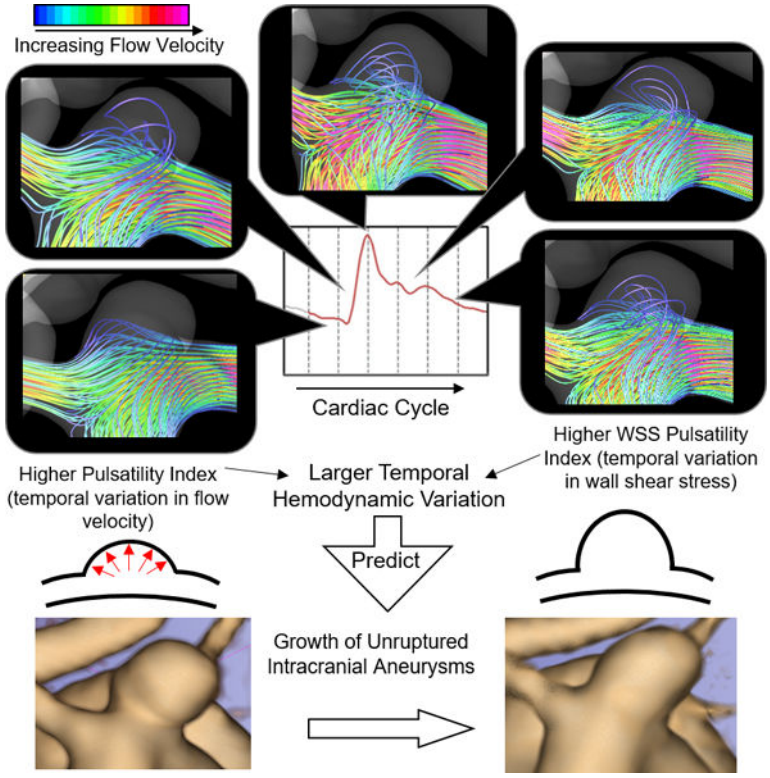

Keywords

Intracranial Aneurysm Growth; Pulsatility Index; Wall Shear Stress Pulsatility Index; Hemodynamic Imbalance; Size Ratio; Computation Fluid Dynamics

INTRODUCTION

Due to their asymptomatic nature, unruptured intracranial aneurysms (IA) are difficult to detect through physical exams and are often incidentally discovered in medical images. Once found, an IA's prospective trajectory is important to consider when devising a treatment plan as the outcome can be as serious as a fatal subarachnoid hemorrhage.[1] However, as the pathophysiology of IA has yet to be elucidated, clinical decision-making currently relies largely on image-derived metrics.[2] This has prompted investigations for predictors of IA rupture employing image-based segmentation techniques, which allow researchers to closely examine the biomechanics of IA pathogenesis with morphological analysis and computational fluid dynamics (CFD) simulations. Over the past decade, several morphological and hemodynamic metrics have been consistently linked to IA rupture, including size ratio (SR), non-sphericity index (NSI), wall shear stress (WSS), and pulsatility index (PI).[3–12]

While predictors of IA rupture have been well studied, current knowledge regarding image-derived predictors of IA growth in unruptured IA cases is limited. Most prior research on IA growth has focused on demographic, genetic, and lifestyle-related factors.[13–18] Among the few studies that have tested image-derived metrics as potential factors to differentiate growing and stable IAs, findings have been inconsistent. Some studies yielded evidence for aspect ratio, SR, NSI, WSS, and flow velocity gradients to be related to IA growth.[3,19–24] Yet, other studies reported that none of the tested metrics could foretell IA growth.[25,26] Further, PI and wall shear stress pulsatility index (WSSPI) are important indices quantifying temporal hemodynamic instability that have been linked to risk of IA rupture.[6,8] However, these parameters have not been studied as predictors of IA growth.

In general, IA growth has been less studied than IA rupture. This could be attributed to the fact that the two processes are thought to be mechanically similar as IA growth has been associated with eventual rupture.[27,28] However, growing IAs do not always rupture, and IAs can rupture without further growth (for example small IAs may rupture without growing bigger).[29,30] While evidence supports the association of the two, the underlying pathologies are likely distinct. In order to accurately predict the trajectory of an IA, dedicating adequate attention to both processes and may be important.

Additional research is warranted to understand IA growth. In this study, we investigate IA growth using real-patient data, and we combine imaged-derived and pulsatile-based simulation techniques to revisit several important morphological and hemodynamic indices, including PI and WSSPI, within a group unruptured IAs. Our goal is to verify metrics that can be clinically useful for predicting growth risks in incidentally found IAs and further elucidate the underlying mechanism of IA growth. We hypothesize that indices that have been previously linked to IA rupture would also be related to IA growth.

METHODS

Case Selection and Growth Status Criteria

This study was approved by the UCLA Institutional Review Board. The TRIPOD checklist for studies developing a prediction model was employed. Due to the sensitive nature of the data collected for this study and to protect patient privacy, requests to access the data by researchers trained in human subject research may be sent to the corresponding author. IA cases were pooled from UCLA Medical Center's clinical electronic records over the period of 2018–2020. Patients with at least 3 follow-up imaging studies were reviewed in order to confirm the growth status of IAs. Furthermore, images with adequate resolution for granular modeling of hemodynamic profiles were selected. IA cases were assigned to stable or growing groups based on their trajectory since detection. Due to the diversity of aneurysm sizes in our sample, we did not set an absolute diameter change threshold to determine an IA's growth status. Rather, cases with an overall increase in diameter of 10% or more from initial to final images were considered growing. Diameter was defined as the maximum distance of an aneurysm.

After reviewing 108 images, we found a total of 36 unruptured IA cases, 20 with known prospective growth and 16 with known prospective stable trajectory. Mean and standard

deviation of follow up were 24.5±6.5 months for the stable group and 25.3±8.7 months for the growing group. A variety of baseline parameters were recorded for these IA cases, including anatomical location, multiplicity, patient gender, race, history of smoking, and history of subarachnoid hemorrhage. Pearson chi-square or exact tests were employed to ensure baseline similarity of these variables between stable and growing IAs (Table 1).

Vascular Reconstruction Model and Computational Fluid Dynamic Analysis

Vascular models of IA cases were manually constructed by a single operator using patient specific CFD simulation software.[31] The earliest image of each case, prior to growth or stable trajectories, was employed for modeling. As MRA images were shown to be highly effective in detecting IA enlargement, vascular structures of most IA cases (11 stable cases and 16 growing cases) were reconstructed using MRA images.[32] CTA images were used for Anterior Communicating Artery (ACOM) cases (5 stable cases and 4 growing cases) due to higher spatial resolution near the communication region of Anterior Cerebral Arteries. We also employed geodesic techniques to verify resolution of segmentation models, which was shown to enable accurate characterization of vessel morphology despite lower spatial resolutions of MRA and CTA images compared to 3DRA images.[33,34]

Inlets were simulated from left cavernous Internal Carotid Arteries (ICA), right cavernous ICA, and Basilar Artery, to the entire Circle of Willis. Inflow arteries were extruded based on patient-specific boundary conditions. Vascular structures were reconstructed from inflow arteries until at least 10 mm past Middle Cerebral Artery (MCA) bifurcations, ACOM, and Posterior Cerebral Artery (PCA) P2. Outflow arteries were also extruded according to patient-specific conditions to minimize boundary effects.[33]

Adjusted patient-specific flow profiles adapted from real cerebral blood flow measurements were constructed based on vessel morphology and size utilizing phase-contrast MR imaging.[31,35] Unsteady 3D Navier-Strokes equations with incompressible Newtonian fluid (attenuation=1.0g/cm^3, viscosity=0.4 poise) were modeled for calculation of flow velocity, pressure, and WSS distribution. Two cardiac cycles, with 100 steps per cycle, were simulated.[36]

Data Extraction

We adapted a previously developed plane-based data extraction approach. For each IA, hemodynamic data was recorded at 5 locations: inflow artery, outflow artery, and three parallel planes (neck, body, dome) that evenly divided an aneurysm into three segments.[31] First, a plane that perpendicularly cuts through the neck region of an aneurysm was identified. Subsequently, two additional planes, exactly parallel to the initial plane and evenly apart, were generated by the software, forming the aneurysm body and dome planes. Inflow and outflow planes were generated as planes perpendicular to the lateral walls of aneurysms that cut through inflow and outflow arteries.[31]

Although this extraction method simplifies the hemodynamics of an aneurysm, it was previously shown to capture similar hemodynamic profiles as methods with increased granularity over entire aneurysms.[31] As simulated flow is continuous throughout an

aneurysm, the quantitative shifts and hemodynamic characteristics throughout aneurysms are adequately captured by this technique.

Candidate Predictors of Intracranial Aneurysm Growth

Image-derived indices examined in this study were adapted from Chien[8] and Geers[37], including time-averaged flow rate (TAFR), PI, time-averaged WSS (TAWSS), WSSPI, normalized, maximum, and minimum WSS ratios, aspect ratio, SR, NSI, volume ratio, and surface ratio. Index formulas are detailed in Appendix 1.

Spatial WSS gradients have been shown to be important in mechanisms of IA development.[37] In this study, we aim to capture macroscopic variations in hemodynamics over an entire aneurysm. To accomplish this, flow data from the aneurysm neck, body, and dome regions were collectively evaluated to determine spatial variations in intra-aneurysmal FR and WSS. The degrees of variations were quantified using calculated mean deviations of time-averaged flow data across those 3 locations. These values will be referred to as intrasaccular spatial FR deviation (ISFRD) and intrasaccular spatial WSS deviation (ISWSSD).

$$Intrasaccular\ Spatial\ Flow\ Rate\ Deviation\ (ISFRD) = \frac{1}{3}\sum_{i=1}^{3}\frac{\left|TAFR_i - \overline{TAFR}\right|}{\overline{TAFR}}$$

1=neck, 2=body, 3=dome

$$Intrasaccular\ Spatial\ Wall\ Shear\ Stress\ Deviation\ (ISWSSD) = \frac{1}{3}\sum_{i=1}^{3}\frac{\left|TAWSS_i - \overline{TAWSS}\right|}{\overline{TAWSS}}$$

1=neck, 2=body, 3=dome

Statistical Analysis

Pearson Chi-square or Fisher's Exact tests were employed to compare background variables such as patient gender, race, history of smoking, history of subarachnoid hemorrhage, aneurysm location, diameter, and multiplicity between stable and growing IAs to ensure baseline similarity.

Analysis of variance (ANOVA) was performed to quantify differences in index values between growing and stable IAs. Since size is a known risk factor of IA growth, additional analysis controlling for aneurysm diameter was performed for all indices with $p<0.10$ from ANOVA. Specifically, analysis of covariance (ANCOVA) was performed with growth status as the fixed factor, aneurysm diameter as the covariate, and index value as the dependent variable. Homogeneity of variance and regression and linearity conditions were met for all ANCOVA tests. Furthermore, interaction between growth status and image modality was assessed for each significant index to rule out image modality as a potential source of bias.

Finally, statistically significant indices from either ANOVA or ANCOVA were entered as covariates into a stepwise multiple logistic regression model with IA growth as the outcome variable to compute the prediction power of these indices. Receiver operation characteristics (ROC) analysis was performed to obtain performance measures. Statistical significance was assessed at two-tailed, α=0.05.

RESULTS

A summary of background variables is presented in Table 1. The growing group consisted of 35% ICA, 35% MCA, 20% ACOM, and 10% Basilar IAs. The stable group consisted of 37.5% ICA, 12.5% MCA, 31.25% ACOM, 12.5% posterior communicating artery (PCOM), and 6.35% Basilar IAs. In both groups, most participants were females of Caucasian descent with no history of subarachnoid hemorrhage. Around half of participants in both groups had a history of tobacco usage (56.25% among stable IAs and 40% among growing IAs). Bivariate tests revealed that all background variables were not significantly different between stable and growing IAs, albeit multiplicity status approached statistical significance.

Figure 1 illustrates results from hemodynamic simulations and Table 2 summarizes index values and statistical test results. Compared to stable IAs, growing IAs exhibited significantly higher PI_{neck} (p=0.048), PI_{body} (p=0.004), ISFRD (p=0.023), $WSSPI_{inflow}$ (p=0.041), $WSSPI_{body}$ (p=0.015), $WSSPI_{dome}$ (p=0.009), and ISWSSD (p=0.006). All other hemodynamic parameters were not significantly different between stable and growing IAs. After controlling for aneurysm diameter, PI_{body} (F=8.71, p=0.003, η^2=0.23), PI_{dome} (F=8.04, p=0.008, η^2=0.20), ISFRD (F=6.01, p=0.020, η^2=0.15), $WSSPI_{body}$ (F=8.47, p=0.006, η^2=0.20), $WSSPI_{dome}$ (F=11.08, p=0.002, η^2=0.25), and ISWSSD (F=6.77, p=0.014, η^2=0.17) were significantly higher among growing IAs. SR (p=0.021) was significantly higher among growing IAs. However, after adjustment of aneurysm diameter, SR was not significantly different between growing and stable IAs (p=0.143).

Among indices that were significantly different between growing and stable IAs, no significant interaction between growth status and image modality was found except for $WSSPI_{body}$ (p=0.049) and SR (p=0.017). For both interactions, growth was associated with higher index values regardless of image modality as significant main effects of growth status on both $WSSPI_{body}$ and size ratio were observed (F=11.21, p=0.002, η^2=0.26; F=15.33, p<0.001, η^2=0.34,); growing aneurysms exhibited significantly higher $WSSPI_{body}$ and size ratio compared to stable aneurysms. The interaction was significant because the association between growth status and index values were stronger among CTA (ACOM only) cases than MRA cases (Figure 2).

In stepwise multiple logistic regression analysis, PI_{body}, $WSSPI_{inflow}$, and $WSSPI_{body}$ predicted IA growth with an overall accuracy of 88.2%: $\text{logit(growth)} = 2.035 \times PI_{body} + 14.004 \times WSSPI_{inflow} + 4.263 \times WSSPI_{body} - 17.342$. ROC analysis revealed an AUC of 0.94. (p<0.0001; Table 3, Figure 3)

DISCUSSION

Our findings showed that higher intra-aneurysmal PIs, ISFRD, $WSSPI_{inflow}$, $WSSPI_{body}$, $WSSPI_{dome}$, ISWSSD, and SR were associated with elevated risks of IA growth. After controlling for aneurysm diameter, PI and WSSPI at aneurysm body and dome, ISFRD, and ISWSSD were still significantly associated with IA growth. A stepwise logistic regression model that considers PI_{body}, $WSSPI_{inflow}$, and $WSSPI_{body}$ altogether predicted IA growth with an 88.2% accuracy in our sample.

Hemodynamic Parameters as Candidate Predictors of Growth

Similar to several prior investigations, we also did not find significant differences in WSS ratios and time averaged WSS between stable and growing IAs.[4,7,9,12] As proposed by Meng et al.[7], high WSS and low WSS elicit separate pathways which can both result in aneurysm growth. Our sample likely included a mixture of growing IAs under the high-WSS pathway and growing IAs under the low-WSS pathway, thereby obscuring a clear difference in WSS between growing and stable IAs. Thus, our finding suggests that WSS alone is likely not a reliable predictor of IA growth.

Instead, WSSPI and ISWSSD, indices quantifying temporal and spatial variations in WSS, were robust predictors of IA growth in our study, even after controlling for aneurysm size. Meng et al.[7] previously suggested that aberrant WSS conditions, as opposed to high or low WSS, drive aneurysm growth by facilitating destructive changes in the extracellular matrix. Since we observed significance only in WSS indices that assess hemodynamic instability, our finding corroborates Meng's theory. Temporal and spatial gradients in WSS magnitude were previously shown to be closely linked to mechanisms of IA initiation.[37] A previous CFD study also found that IA growth was associated with complex intra-aneurysmal hemodynamic patterns which elicit uneven, fluctuating WSS profiles.[19] Our study adds that this irregular WSS distribution can be characterized in multiple forms. Namely, both high degrees of WSS variations spatially and temporally were linked to IA growth.

Our finding also showed that temporal variations in flow rates were strongly predictive of IA growth. Previous studies have found higher PI, especially at the neck region, to associate with higher risks of rupture.[6,8] While few to no CFD studies have examined PI's relationship with IA growth, our finding suggests that higher PI is also linked to elevated risks of IA growth. It has been previously argued that large aneurysm size elicits higher PI due to cerebral aneurysms' Windkessel effect on distal arteries, where the aneurysm serves as a reservoir for blood during systole and releases blood during diastole.[38] We found that higher PI at the aneurysm neck region was associated with higher risks of IA growth, but this relationship was no longer significant when aneurysm size was accounted for. However, high PI at saccular regions of aneurysms still reliably predicted IA growth despite adjustment for aneurysm size. Therefore, our findings suggest that the link between PI at the neck region and IA growth may be related to aneurysm size and mediated by the Windkessel effect (larger aneurysm size leads to larger PI at the neck region). Meanwhile, the link between PI at saccular regions and IA growth may be less related to aneurysm size and the Windkessel effect. Nevertheless, we found that higher PI is strongly associated with elevated risks of IA growth. PI quantifies the changes in FR over a cardiac cycle. As a high PI value is typically

understood as a marker of distal resistance in blood vessels, it may highlight important biomechanical features related to IA pathophysiology.[39]

Additionally, we found ISFRD, which quantifies spatial variation in intra-aneurysmal FRs, to be associated with IA growth, even after adjustment for aneurysm size. A recent CFD study discovered that cerebral aneurysm growth tends to occur in areas of high velocity gradient between aneurysmal wall and swirling flow structures.[21] Although ISFRD encapsulates the macroscopic flow velocity changes over an aneurysm, our observation similarly suggests that spatial FR fluctuations are related to mechanisms of IA growth.

Upon examination of hemodynamic characteristics, we found that metrics indicative of hemodynamic imbalance consistently predicted IA growth. In fact, when examining temporal variations in both FR and WSS (PI and WSSPI) together, prediction of IA growth can be as accurate as 88%. Vascular remodeling as an adaptive response to hemodynamic imbalance is fundamental to the pathophysiology of intracranial anuerysm.[40] It is likely that hemodynamic instability caused by WSS and FR variations perpetuate further vascular remodeling beyond IA initiation, resulting in IA growth. In fact, high WSS gradients were hypothesized to promote aneurysm growth by facilitating mural cells' production of matrix metalloproteinase, which stimulates medial thinning and mural cell apoptosis.[6] This proposed pathway can potentially explain the consistent link between variables related to hemodynamic imbalance and IA growth in the present study.

Morphologic Parameters as Candidate Predictors of Growth

Furthermore, SR, the ratio between aneurysm maximum height and average parent artery diameter, was associated with IA growth in our sample. Many large-scale studies in the past have also found higher SR to be linked to risks of IA growth and rupture.[3,4,11,12,20] Specifically, a high SR was shown to be indicative of aneurysm shape that is prone to evoke multiple intra-aneurysmal flow vortices and complex flow patterns that are linked to IA rupture.[41] Our findings suggest that similar complex flow patterns may also be perpetuating IA growth as aberrant hemodynamics associated with high SR morphology likely propels vascular remodeling and pathogenesis of IA growth.[40] This is consistent with our study finding that hemodynamic imbalance predisposes IAs to risks of further development.

NSI was previously found to be a predictor of IA rupture.[4,8] In a recent study, NSI was also shown to be a predictor of growth for IAs with initial diameters of below 5 mm or above 7 mm.[20] While we also found a trend of higher NSI among growing IAs compared to stable IAs, this trend was not as clear, likely because size-dependent analyses were not performed. Although our sample included IAs of diverse sizes, we opted not to further segregate IAs into subcategories by size since the resulting low case numbers would render statistical comparisons prone to biases. NSI should be further explored in larger cohorts in the future.

Limitations

While our study provides compelling evidence for the link between hemodynamic aberrance and IA growth, several limitations should be noted. Multiplicity status may serve as a potential confounding variable to our findings as bivariate analysis revealed a difference between growing and stable IAs that approached statistical significance. However, IAs in

patients with multiple aneurysms were previously shown to be more likely to grow.[15] As the growing group in our sample included a lower proportion of IAs from patients with multiple IAs, we do not believe our finding was heavily influenced by this variable.

Furthermore, multiple image modalities, CTA and MRA, were employed for vascular model segmentation. However, since CTA images were only employed for ACOM cases, which were relatively evenly distributed among growing and stable groups, the risk of bias due to image modality is low. Further tests using ANOVA showed that in this cohort there was no significant hemodynamic difference due to aneurysm location for PI and WSSPI parameters except for $WSSPI_{dome}$. Additionally, we conducted interaction analyses specifically to address this concern and only found image modality to interact with growth status for 2 index values, SR and $WSSPI_{body}$. Among those interactions, our major findings were also showed unaffected by image modality as SR and $WSSPI_{body}$ index values were much higher among growing IAs regardless of image modality. The interactions were significant because the associations between IA growth and index values were stronger among CTA cases than MRA cases. Nevertheless, since the direction of relationship between index values and IA growth remains the same regardless of image modality, our use of both MRA and CTA images likely did not impact the major implications of our findings.

Finally, PI and WSSPI can be affected by physiological factors such as blood pressure, heart rate, and vascular compliance. The current model adapted the flow waveforms collected from normal cerebral arteries and then scaled them based on patient-specific inflow conditions. This standardized method is used by many research groups to make hemodynamic comparison feasible, whereas individual patient cerebral flow profiles and blood flow pressure may vary during measurements and daily activities.[4,31,35] While we have highlighted important relationships between pulsatile-based metrics and IA growth, future investigations may benefit from explicitly incorporating patient-specific measurements of these physiological factors into the simulation model.

Despite these potential limitations, with a well-distributed sample of IAs from diverse anatomical locations, our analysis, to our knowledge, is the first to elucidate the robust roles of PI and WSSPI in predicting IA growth. These indices are important to report in the literature for further investigation of their pathophysiological implications and development of clinical applications.

CONCLUSIONS

Metrics indicating large degrees of temporal and spatial hemodynamic variations reliably differentiated growing and stable IAs in our study, even after controlling for morphological parameters. Specifically, collective evaluation of PI and WSSPI index values accurately predicted IA growth in our sample. Upon further study, these parameters may aid understanding of IA pathophysiology and early identification of IA's growth trajectories.

Supplementary Material

Refer to Web version on PubMed Central for supplementary material.

ACKNOWLEDGMENTS

The authors have no conflict of interest to disclose.

SOURCES of FUNDING

This research is in part supported by NIH R01HL152270; AHA Innovative Project Award 18IPA34170130, and an UCLA Exploratory Research Grant.

Abbreviations

CFD	computational fluid dynamics
IA	intracranial aneurysm
PI	pulsatility index
WSS	wall shear stress
SR	size ratio
NSI	non-sphericity index
FR	flow rate
TA	time-averaged
ISFRD	intrasaccular spatial flow rate deviation
ISWSSD	intrasaccular spatial wall shear stress deviation
ICA	Internal Carotid Artery
MCA	Middle Cerebral Artery
ACOM	Anterior Communicating Artery
PCA	Posterior Cerebral Artery
PCOM	Posterior Communicating Artery

References

1. Brown RD. Unruptured intracranial aneurysms. Seminars in Neurology 2010;30:537–544. [PubMed: 21207346]
2. Rikhtegar R, Mosimann PJ, Rothaupt J, Mirza-Aghazadeh-Attari M, Hallaj S, Yousefi M, Amiri A, Farashi E, Kheyrollahiyan A, Dolati S. Non-coding RNAs role in intracranial aneurysm: General principles with focus on inflammation. Life Sciences 2021;278:119617. [PubMed: 34004250]
3. Jirjees S, Htun ZM, Aldawudi I, Katwal PC, Khan S. Role of Morphological and Hemodynamic Factors in Predicting Intracranial Aneurysm Rupture: A Review. Cureus 2020;12:e9178. [PubMed: 32802613]
4. Xiang J, Natarajan SK, Tremmel M, Ma D, Mocco J, Hopkins LN, Siddiqui AH, Levy EI, Meng H. Hemodynamic-morphologic discriminants for intracranial aneurysm rupture. Stroke 2011;42:144–152. [PubMed: 21106956]
5. Chien A, Sayre J, Viñuela F. Comparative morphological analysis of the geometry of ruptured and unruptured aneurysms. Neurosurgery 2011;69:349–356. [PubMed: 21415785]

6. Patti J, Viñuela F, Chien A. Distinct trends of pulsatility found at the necks of ruptured and unruptured aneurysms. Journal of Neurointerventional Surgery 2014;6:103–107. [PubMed: 23416784]
7. Meng H, Tutino VM, Xiang J, Siddiqui A. High WSS or Low WSS? Complex interactions of hemodynamics with intracranial aneurysm initiation, growth, and rupture: Toward a unifying hypothesis. American Journal of Neuroradiology 2014;35:1254–1262. [PubMed: 23598838]
8. Chien A, Sayre J. Morphologic and hemodynamic risk factors in ruptured aneurysms imaged before and after rupture. American Journal of Neuroradiology 2014;35:2130–2135. [PubMed: 24970547]
9. Zhang Y, Yang X, Wang Y, Liu J, Li C, Jing L, Wang S, Li H. Influence of morphology and hemodynamic factors on rupture of multiple intracranial aneurysms: Matched-pairs of ruptured-unruptured aneurysms located unilaterally on the anterior circulation. BMC Neurology 2014;14:253. [PubMed: 25551809]
10. Liu J, Fan J, Xiang J, Zhang Y, Yang X. Hemodynamic characteristics of large unruptured internal carotid artery aneurysms prior to rupture: A case control study. Journal of NeuroInterventional Surgery 2016;8:367–372. [PubMed: 25653231]
11. Mocco J, Brown RD, Torner JC, Capuano AW, Fargen KM, Raghavan ML, Piepgras DG, Meissner I, Huston J, International Study of Unruptured Intracranial Aneurysms Investigators. Aneurysm morphology and prediction of rupture: An international study of unruptured intracranial aneurysms analysis. Neurosurgery 2018;82:491–496. [PubMed: 28605486]
12. Lv N, Karmonik C, Chen S, Wang X, Fang Y, Huang Q, Liu J. Wall Enhancement, Hemodynamics, and Morphology in Unruptured Intracranial Aneurysms with High Rupture Risk. Translational Stroke Research 2020;11:882–889. [PubMed: 31960286]
13. Villablanca JP, Duckwiler GR, Jahan R, Tateshima S, Martin NA, Frazee J, Gonzalez NR, Sayre J, Vineula FV. Natural history of asymptomatic unruptured cerebral aneurysms evaluated at CT angiography: Growth and rupture incidence and correlation with epidemiologic risk factors. Radiology 2013;269:258–265. [PubMed: 23821755]
14. Brinjikji W, Pereira VM, Khumtong R, Kostensky A, Tymianski M, Krings T, Radovanovich I. PHASES and ELAPSS Scores Are Associated with Aneurysm Growth: A Study of 431 Unruptured Intracranial Aneurysms. World Neurosurgery 2018;114:e425–e432. [PubMed: 29530704]
15. Chien A, Callender RA, Yokota H, Salamon N, Colby GP, Wang AC, Szeder V, Jahan R, Tateshima S, Villablanca J, et al. Unruptured intracranial aneurysm growth trajectory: Occurrence and rate of enlargement in 520 longitudinally followed cases. Journal of Neurosurgery 2019;132:1077–1087. [PubMed: 30835694]
16. Jin D, Song C, Leng X, Han P. A systematic review and meta-analysis of risk factors for unruptured intracranial aneurysm growth. International Journal of Surgery 2019;69:68–76. [PubMed: 31356963]
17. Serrone JC, Tackla RD, Gozal YM, Hanseman DJ, Gogela SL, Vuong SM, Kosty JA, Steiner CA, Krueger BM, Grossman AW, et al. Aneurysm growth and de novo aneurysms during aneurysm surveillance. Journal of Neurosurgery 2016;125:1374–1382. [PubMed: 26967775]
18. Chien A, Liang F, Sayre J, Salamon N, Villablanca P, Vinuela F. Enlargement of small, asymptomatic, unruptured intracranial aneurysms in patients with no history of subarachnoid hemorrhage: the different factors related to the growth of single and multiple aneurysms. Journal of Neurosurgery 2013;119:190–197. [PubMed: 23621603]
19. Sforza DM, Kono K, Tateshima S, Viñuela F, Putman C, Cebral JR. Hemodynamics in growing and stable cerebral aneurysms. Journal of Neurointerventional Surgery 2016;8:407–412. [PubMed: 25653228]
20. Chien A, Xu M, Yokota H, Scalzo F, Morimoto E, Salamon N. Nonsphericity index and size ratio identify morphologic differences between growing and stable aneurysms in a longitudinal study of 93 cases. American Journal of Neuroradiology 2018;39:500–506. [PubMed: 29371255]
21. Nordahl ER, Uthamaraj S, Dennis KD, Sejkorova A, Hejcl A, Hron J, Svihlova H, Carlson KD, Suzen YB, Dragomir-Daescu D. Morphological and hemodynamic changes during cerebral aneurysm growth. Brain Sciences 2021;11:520. [PubMed: 33921861]

22. Khan MO, Arana VT, Rubbert C, Cornelius JF, Fischer I, Bostelmann R, Mijderwijk H, Turowski B, Steiger H, May R, et al. Association between aneurysm hemodynamics and wall enhancement on 3D vessel wall MRI. Journal of Neurosurgery 2020;134:565–575.

23. Zhang X, Karuna T, Yao ZQ, Duan C, Wang X, Jiang S, Li X, Yin J, He X, Guo S, et al. High wall shear stress beyond a certain range in the parent artery could predict the risk of anterior communicating artery aneurysm rupture at follow-up. Journal of Neurosurgery 2019;131:868–875.

24. Cornelissen BMW, Schneiders JJ, Potters WV, Berg RVD, Velthuis BK, Rinkel GJE, Slump CH, VanBavel E, Majoie CBLM, Marquering HA. Hemodynamic differences in intracranial aneurysms before and after rupture. American Journal of Neuroradiology 2015;36:1927–1933. [PubMed: 26089313]

25. Ramachandran M, Retarekar R, Raghavan ML, Berkowitz B, Dickerhoff B, Correa T, Lin S, Johnson K, Hasan D, Ogilvy C, et al. Assessment of image-derived risk factors for natural course of unruptured cerebral aneurysms. Journal of Neurosurgery 2016;124:288–295. [PubMed: 26381246]

26. Leemans EL, Cornelissen BMW, Slump CH, Majoie CBLM, Cebral JR, Marquering HA. Comparing Morphology and Hemodynamics of Stable-versus-Growing and Grown Intracranial Aneurysms. American Journal of Neuroradiology 2019;40:2102–2110. [PubMed: 31780462]

27. Jing L, Fan J, Wang Y, Li H, Wang S, Yang X, Zhang T. Morphologic and hemodynamic analysis in the patients with multiple intracranial aneurysms: Ruptured versus unruptured. PLoS ONE 2015;10:e0132494. [PubMed: 26147995]

28. Backes D, Rinkel GJE, Laban KG, Algra A, Vergouwen MDI. Patient-and aneurysm-specific risk factors for intracranial aneurysm growth: A systematic review and meta-analysis. Stroke 2016;47:951–957. [PubMed: 26906920]

29. Growth Juvela S. and rupture of unruptured intracranial aneurysms. Journal of Neurosurgery 2018;131:843–851. [PubMed: 30215563]

30. Chmayssani M, Rebeiz JG, Rebeiz TJ, Batjer HH, Bendok BR. Relationship of growth to aneurysm rupture in asymptomatic aneurysms ≤ 7 mm: A systematic analysis of the literature. Neurosurgery 2011;68:1164–1171.

31. Chien A, Castro MA, Tateshima S, Sayre J, Cebral J, Viñuela F. Quantitative hemodynamic analysis of brain aneurysms at different locations. American Journal of Neuroradiology 2009;30:1507–1512. [PubMed: 19406766]

32. Nakagawa D, Nagahama Y, Policeni BA, Raghavan ML, Dillard SI, Schumacher AL, Sarathy S, Dlouhy BJ, Wilson S, Allan L, et al. Accuracy of detecting enlargement of aneurysms using different MRI modalities and measurement protocols. Journal of Neurosurgery 2018;130:559–565. [PubMed: 29521585]

33. Chien A, Viñuela F. Analyzing Circle of Willis blood flow in ischemic stroke patients through 3D Stroke Arterial Flow Estimation. Interventional Neuroradiology 2017;23:427–432. [PubMed: 28530158]

34. Yang X, Cheng KTT, Chien A. Geodesic active contours with adaptive configuration for cerebral vessel and aneurysm segmentation In: Proceedings - International Conference on Pattern Recognition. 2014.

35. Mut F, Löhner R, Chien A, Tateshima S, Vinuela F, Putman C, Cebral J. Computational hemodynamics framework for the analysis of cerebral aneurysms. International Journal for Numerical Methods in Biomedical Engineering 2011;27:822–839. [PubMed: 21643491]

36. Chien A, Sayre J, Viñuela F. Quantitative comparison of the dynamic flow waveform changes in 12 ruptured and 29 unruptured ICA-ophthalmic artery aneurysms. Neuroradiology 2013;55:313–320. [PubMed: 23443738]

37. Geers AJ, Morales HG, Larrabide I, Butakoff C, Bijlenga P, Frangi AF. Wall shear stress at the initiation site of cerebral aneurysms. Biomechanics and Modeling in Mechanobiology 2017;16:97–115. [PubMed: 27440126]

38. Hussein AE, Brunozzi D, Shakur SF, Ismail R, Charbel FT, Alaraj A. Cerebral aneurysm size and distal intracranial hemodynamics: An assessment of flow and pulsatility index using quantitative magnetic resonance angiography. Neurosurgery 2018;83:660–665. [PubMed: 28945889]

39. Wielicka M, Neubauer-Geryk J, Kozera G, Bieniaszewski L. Clinical application of pulsatility index. Medical Research Journal 2020;5:201–210.

40. Hashimoto T, Meng H, Young WL. Intracranial aneurysms: Links among inflammation, hemodynamics and vascular remodeling. Neurological Research 2006;28:372–380. [PubMed: 16759441]

41. Tremmel M, Dhar S, Levy EI, Mocco J, Meng H. Influence of intracranial aneurysm-to-parent vessel size ratio on hemodynamics and implication for rupture: Results from a virtual experimental study. Neurosurgery 2009;64:622–630. [PubMed: 19349824]

CLINICAL PERSPECTIVES

What is new?

- High pulsatility index, wall shear stress pulsatility index, and intrasaccular location-dependent hemodynamic variations are shown to be predictive of intracranial aneurysm growth.

What are the clinical implications?

- Temporal and spatial hemodynamic instability may be involved in the mechanism and pathophysiology of intracranial aneurysm growth.
- Predictors of aneurysm growth highlighted in this study may aid in clinical risk assessment.

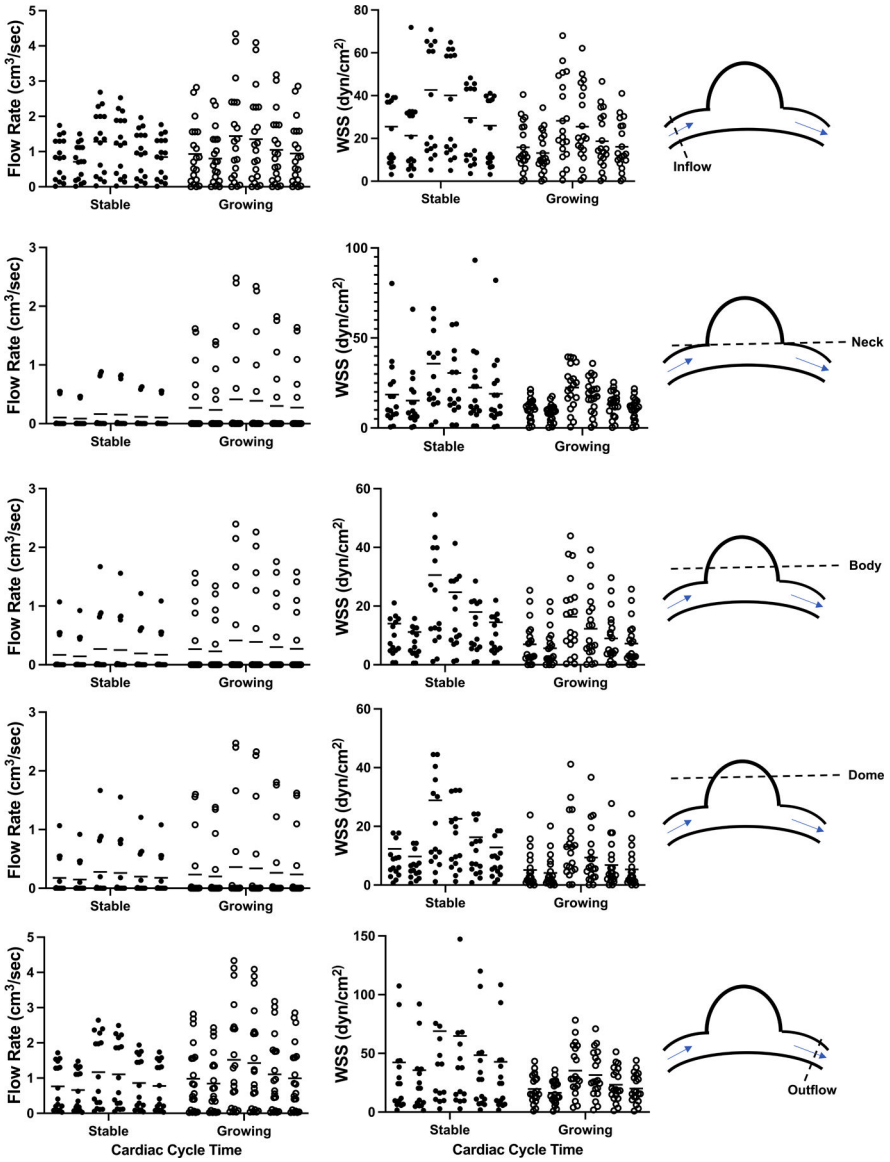

Figure 1. Scatter Plots of Pulsatile Flow Rates and Wall Shear Stress Over a Cardiac Cycle among Stable and Growing Cases.

Bars represent average values within the group of cases at that particular time point. Results from flow simulations were calculated at 6 specific timepoints, which correspond to the 6 timepoints presented in this figure. At each timepoint, calculations were performed at 5 specific locations for each aneurysm: inflow artery, aneurysm neck, aneurysm body, aneurysm dome, and outflow artery, as depicted in the figure. WSS=wall shear stress.

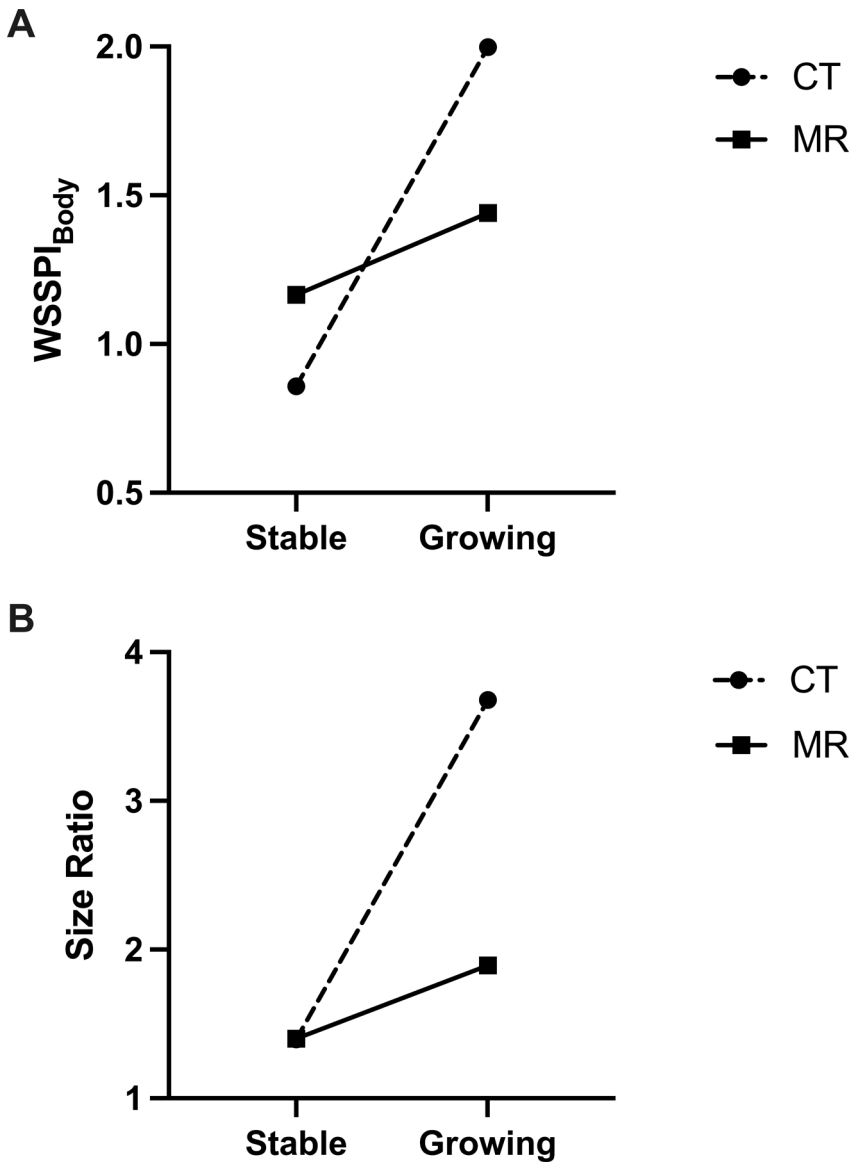

Figure 2. Line Graphs Illustrating Significant Interactions between Image Modality and Growth Status for WSSPI at Aneurysm Body (A) and Size Ratio (B).

Analysis of Covariance (ANCOVA) revealed significant interactions between image modality and growth status when wall shear stress pulsatility index (WSSPI) at aneurysm body and size ratio were treated as dependent variables ($F=4.19$, $p=0.049$; $F=6.36$, $p=0.017$, respectively). Further, there was a significant main effect of growth status on $WSSPI_{body}$ ($F=11.21$, $p=0.002$) and significant main effects of both image modality and growth status on size ratio ($F=6.31$, $p=0.018$; $F=15.33$, $p<0.001$, respectively).

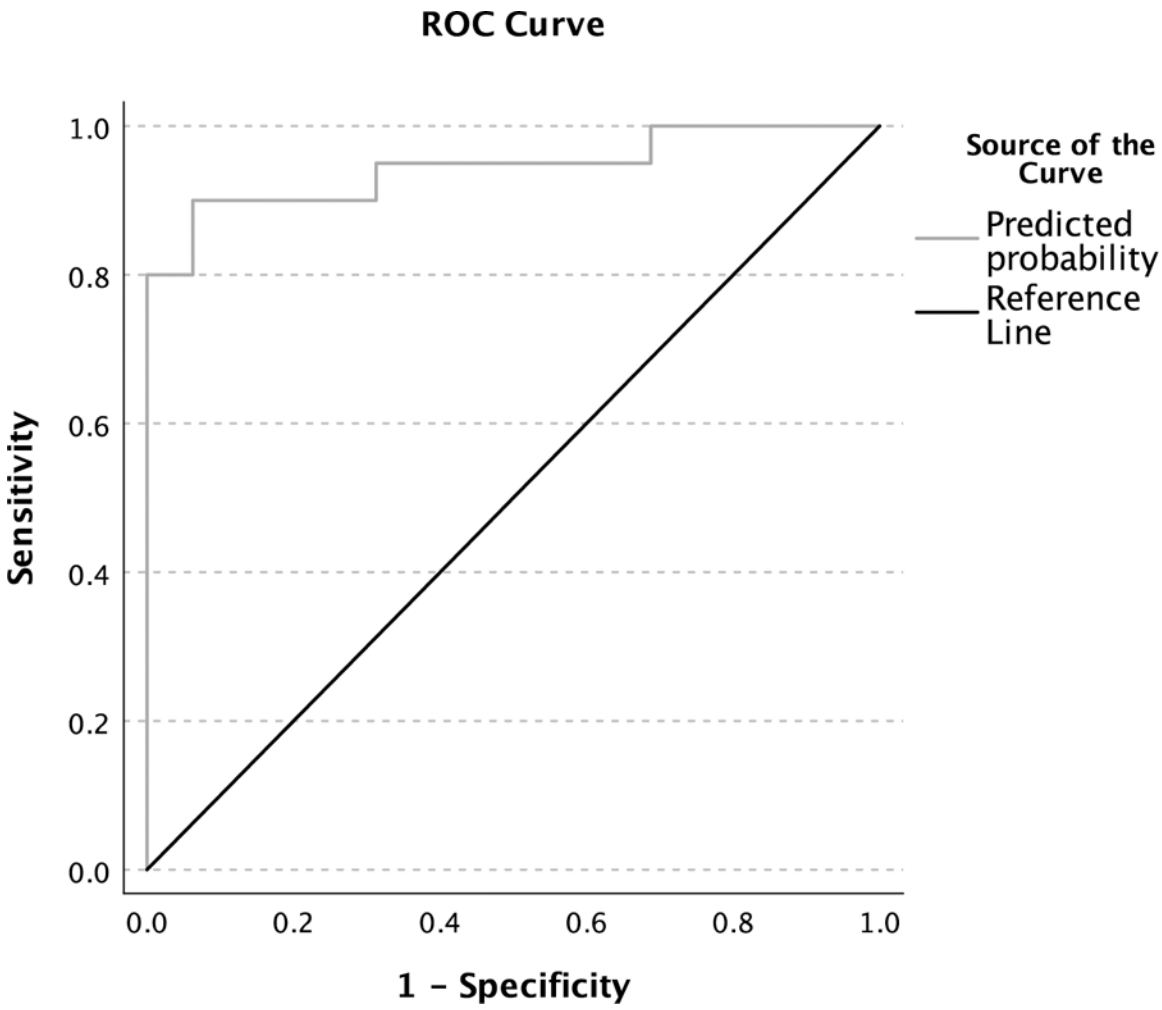

Figure 3. ROC Curve Performance Measure of Stepwise Logistic Regression Predictive Model.
Performance measure of the prediction model involving pulsatility index at aneurysm body, wall shear stress pulsatility index at inflow artery, and wall shear stress pulsatility index at aneurysm body. ROC= receiver operating characteristics.

Table 1:

Background Information of Intracranial Aneurysm Cases

	Stable		Growing		Bivariate Tests
	Patients	**Aneurysms**	**Patients**	**Aneurysms**	
Total Count	11 (100%)	16 (100%)	19 (100%)	20 (100%)	-
Location					p=0.338
ICA	-	6 (37.5%)	-	7 (35%)	
ACOM	-	5 (31.25%)	-	4 (20%)	
MCA	-	2 (12.5%)	-	7 (35%)	
Basilar	-	1 (6.25%)	-	2 (10%)	
PCOM	-	2 (12.5%)	-	0 (0%)	
Initial Diameter					-
< 3 mm	-	2 (12.5%)	-	1 (5%)	
3 mm – 5 mm	-	6 (37.5%)	-	7 (35%)	
5 mm – 7 mm	-	4 (25%)	-	1 (5%)	
> 7 mm	-	4 (25%)	-	11 (55%)	
Gender					p=0.113
Male	0 (0%)	0 (0.0%)	4 (21.1%)	4 (20%)	
Female	11 (100%)	16 (100%)	15 (78.9%)	16 (80%)	
Race					p=0.762
Caucasian	8 (72.7%)	10 (62.5%)	10 (52.6%)	10 (50%)	
Asian	1 (9.1%)	3 (18.75%)	3 (15.8%)	3 (15%)	
Hispanic	1 (9.1%)	2 (12.50%)	1 (5.3%)	2 (10%)	
African	0 (0%)	0 (0.00%)	2 (10.5%)	2 (10%)	
Others	1 (9.1%)	1 (6.25%)	3 (15.8%)	3 (15%)	
History of Smoking					p=0.332
Yes	6 (54.5%)	9 (56.25%)	8 (42.1%)	8 (40%)	
No	5 (45.5%)	7 (43.75%)	11 (57.9%)	12 (60%)	
History of SAH					p=0.190
Yes	1 (9.1%)	-	0 (0%)	-	
No	10 (90.9%)	-	19 (100%)	-	
Multiplicity *					p=0.056
Yes	6 (54.5%)	9 (56.25%)	5 (26.3%)	5 (25%)	
No	5 (45.5%)	7 (43.75%)	14 (73.7%)	15 (75%)	

* Multiplicity indicates whether the patient possessed multiple aneurysms. ICA=internal carotid artery. ACOM=anterior communicating artery. MCA=middle cerebral artery. PCOM=posterior communicating artery. SAH=subarachnoid hemorrhage.

Table 2:

Summary of Morphological and Hemodynamic Index Values and Statistics

	Stable (n=16)	Growing (n=20)	ANOVA	ANCOVA (Covariate = Aneurysm Diameter)	Interaction (Growth * Image Modality)
Hemodynamic Parameters					
Time-averaged FR Magnitude (cm^3/sec)					
Inflow	0.97 ± 0.67	1.09 ± 1.01	p=0.687		
Neck	0.12 ± 0.25	0.31 ± 0.62	p=0.255		
Body	0.20 ± 0.38	0.31 ± 0.60	p=0.522		
Dome	0.21 ± 0.37	0.27 ± 0.61	p=0.711		
Outflow	0.89 ± 0.76	1.15 ± 1.11	p=0.438		
Pulsatility Index (PI)					
Inflow	0.60 ± 0.06	0.81 ± 0.61	p=0.178		
Neck	0.78 ± 0.27	1.13 ± 0.65	**p=0.048**	F=3.15, *p*=0.085, η^2=0.09	p=0.13
Body	0.81 ± 0.44	1.76 ± 1.18	**p=0.004**	**F=8.71, *p*=0.003, η^2=0.23**	p=0.51
Dome	1.22 ± 0.76	1.91 ± 1.20	p=0.052	**F=8.04, *p*=0.008, η^2=0.20**	p=0.90
Outflow	0.58 ± 0.07	0.61 ± 0.11	p=0.299		
FR Location-dependent Calculations					
Normalized FR ratio	1.24 ± 2.44	0.66 ± 1.60	p=0.396		
Maximum FR ratio	1.51 ± 3.29	1.47 ± 4.33	p=0.975		
Minimum FR ratio	0.72 ± 1.58	0.17 ± 0.41	p=0.139		
ISFRD	0.43 ± 0.35	0.75 ± 0.44	**p=0.023**	**F=6.01, *p*=0.020, η^2=0.15**	p=0.086 [a]
Time-averaged WSS Magnitude (dyn/cm^2)					
Inflow	30.85 ± 26.13	19.58 ± 13.64	p=0.104		
Neck	23.57 ± 23.79	13.86 ± 7.47	p=0.093	F=2.59, *p*=0.117, η^2=0.07	
Body	18.82 ± 24.78	9.58 ± 8.86	p=0.130		
Dome	17.10 ± 23.37	7.30 ± 7.52	p=0.086	F=2.43, *p*=0.129, η^2=0.07	
Outflow	50.51 ± 67.48	24.40 ± 14.83	p=0.101		
WSS Pulsatility Index (WSSPI)					
Inflow	0.68 ± 0.05	0.87 ± 0.36	**p=0.041**	F=3.35, *p*=0.076, η^2=0.09	p=0.29
Neck	1.02 ± 0.40	1.04 ± 0.30	p=0.870		
Body	1.07 ± 0.22	1.55 ± 0.73	**p=0.015**	**F=8.47, *p*=0.006, η^2=0.20**	**p=0.049**
Dome	1.15 ± 0.30	1.64 ± 0.66	**p=0.009**	**F=11.08, *p*=0.002, η^2=0.25**	p=1.00
Outflow	0.67 ± 0.06	0.82 ± 0.30	p=0.052	F=3.58, *p*=0.067, η^2=0.10	
WSS Location-dependent Calculations					
Normalized WSS ratio	0.53 ± 0.22	0.50 ± 0.36	p=0.805		
Maximum WSS ratio	0.69 ± 0.27	0.76 ± 0.50	p=0.569		
Minimum WSS ratio	0.40 ± 0.24	0.28 ± 0.30	p=0.210		
ISWSSD	0.24 ± 0.20	0.49 ± 0.28	**p=0.006**	**F=6.77, *p*=0.014, η^2=0.17**	p=0.12
Morphological Parameters					
Aneurysm Diameter (mm)	5.21 ± 2.64	8.47 ± 6.19	p=0.058	-	

	Stable (n=16)	Growing (n=20)	ANOVA	ANCOVA (Covariate = Aneurysm Diameter)	Interaction (Growth * Image Modality)
Aspect Ratio	0.72 ± 0.28	0.86 ± 0.30	p=0.173		
Size Ratio (SR)	1.40 ± 0.62	2.27 ± 1.27	**p=0.021**	F=2.26, p=0.143, η^2=0.07	**p=0.017**
Nonsphericity Index (NSI)	0.10 ± 0.06	0.13 ± 0.06	p=0.102		
Volume Ratio	0.44 ± 0.20	0.53 ± 0.25	p=0.250		
Surface Area Ratio	0.50 ± 0.15	0.59 ± 0.19	p=0.142		

FR=flow rate. WSS=wall shear stress. ISFRD=intrasaccular spatial flow rate deviation. ISWSSD=intrasaccular spatial wall shear stress deviation.

Author Manuscript

Author Manuscript

Author Manuscript

Table 3:

Stepwise Multiple Logistic Regression Model and ROC Analysis

	Log odds	Standard Error	Wald	p-value	% Correct Overall Prediction
PI_{body}	2.035	0.896	5.162	0.02	88.2
$WSSPI_{inflow}$	14.004	7.435	3.548	0.06	
$WSSPI_{body}$	4.263	2.405	3.142	0.07	
Constant	−17.342	7.361	5.550	0.02	

Area under the Receiver Operating Characteristic (ROC) Curve *			
Area	**Standard Error**	**Asymptotic Significance†**	**95% Confidence Interval**
0.944	0.039	<0.001	0.867 – 1.021

PI_{body}=pulsatility index at aneurysm body; $WSSPI_{inflow}$=wall shear stress pulsatility index at inflow artery; $WSSPI_{body}$=wall shear stress PI at aneurysm body

*Test result variable: predicted probability from the logistic regression model.

†Null hypothesis: true area=0.5